Effect of roughness and nanoporosity on optical properties of black and reflective Al films prepared by magnetron sputtering

Hruška, P.; More-Chevalier, J.; Novotný, M.; Čížek, J.; Melikhova, O.; Fekete, L.; Poupon, M.; Bulíř, J.; Volfová, L.; Butterling, M.; Liedke, M. O.; Wagner, A.; Fitl, P.;

Originally published:

April 2021

Journal of Alloys and Compounds 872(2021), 159744

DOI: https://doi.org/10.1016/j.jallcom.2021.159744

Effect of roughness and nanoporosity on optical properties of black and reflective Al films prepared by magnetron sputtering

Petr Hruška[1,2,*], Joris More-Chevalier[1], Michal Novotný[1], Jakub Čížek[2], Oksana Melikhova[2], Ladislav Fekete[1], Morgane Poupon[1], Jiří Bulíř[1], Lenka Volfová[1,3], Maik Butterling[4], Maciej Oskar Liedke[4], and Přemysl Fitl[1,5]

[1] Institute of Physics of the Czech Academy of Sciences, Na Slovance 2, 182 21, Prague, Czech Republic
[2] Charles University, Faculty of Mathematics and Physics, V Holešovičkách 2, 180 00 Prague, Czech Republic
[3] Charles University, Faculty of Science, Albertov 6, 128 00 Prague, Czech Republic
[4] Helmholtz-Zentrum Dresden-Rossendorf, Institute of Radiation Physics, Bautzner Landstrasse 400, 01328 Dresden, Germany
[5] University of Chemistry and Technology, Department of Physics and Measurements, Technická 5, 166 28 Prague, Czech Republic

*corresponding author: hruskap@fzu.cz

Keywords: black aluminum, magnetron sputtering, atomic force microscopy, spectrophotometric reflectance, positron annihilation spectroscopy

Abstract

In this work, a comparison of the microstructure of black and classic reflective aluminum films is provided. The N_2 concentration during the magnetron sputtering deposition has a key impact on the growth process and final moth-eye-like morphology of black Al films. The study of films with thickness ~1.5 µm and ~8 µm and fully developed microstructure enabled us to clarify the origin of different optical properties of black and reflective Al. Atomic force microscopy measurements showed high roughnesses for both types of films leading to light scattering from their surface. In the case of black Al, the incident light is absorbed in a fractal-like nanoporous surface. Less than 3 % of the intensity in the wavelength range from 190 nm to 1200 nm is reflected. Positronium formation in columnar nanopores with a diameter of 4 – 5 Å was observed by positron annihilation lifetime spectroscopy. The nanoporosity rather than the roughness is the key feature of black films compared to reflective ones.

1. Introduction

Black metals (BMs) refer to highly porous metals, which can trap light significantly [1]. These porosities are induced during metal growth due to the presence of impurities. The reason that BMs appear "black" is because of their complicated subwavelength electromagnetic interactions with light in wide wavebands [2]. Several techniques have been reported to prepare BMs films like thermal evaporation [3-6], deposition by magnetron sputtering [1, 7, 8], electrodeposition [9-11], thin metal film deposition on dielectric substrates with imprinted antireflective black moth-eye-like nanostructures [12, 13], and laser surface modification [14-17].

To date, BMs have been interesting in different applications like electrochemical sensing, electronics for optical sensing and imaging, solar cells, heat radiator enhancement, catalysis, and energy harvesting [1, 2, 4, 10, 18-21]. Recently, a black aluminum (BAl) coating was utilized for improving the energy conversion from a light source to an electrical current using the pyroelectric effect [22]. Silver nanoplate aggregations exhibited nearly 100 % broadband light antireflective efficiency in the range from 400 nm to 1100 nm and can be useful in various applications, from solar energy harvest, photothermic utility to wide wavelength range antireflection and cloaking [2].

Several metals like gold, platinum, tungsten, copper, titanium, palladium, or aluminum, were investigated to get black or colored [17, 23-29]. BAl owns several advantages, such as good adhesion and good wear resistance. It can also maintain its optical properties at elevated temperatures over 300 °C [6, 30]. Furthermore, BAl is very suitable for industrial utilization due to its low cost. Recently, BAl was simply prepared by direct current (DC) pulsed magnetron sputtering using N_2/Ar mixture with ~6 % of N_2 [1]. At this percentage, the Al film growth process favored the formation of a moth-eye-like antireflective surface. A diffuse reflectance lower than 4 % was reached in the ultraviolet-visible-near infrared (UV-VIS-NIR) spectral range that corresponds to a value observed for ultrahigh absorbers. The columnar film growth model for the Al film in the presence of the N_2 gas has been proposed [1]. However, the role of the N_2 in the BAl film growth has to be specified and structural film analysis, such as positron annihilation spectroscopy analysis, should be performed to clarify the growth mechanism.

Positronium (Ps) is a hydrogen-like bound state of electron and positron [31] with a radius of approximately 1 Å (2 Bohr radii) and is an excellent non-destructive probe of nanoscopic pores in solids [32]. Ps has two states: parapositronium (p-Ps, singlet state, S = 0, opposite spins) and orthopositronium (o-Ps, triplet state, S = 1, parallel spins). In the vacuum, the lifetime of p-Ps is short (125 ps, 2γ self-annihilation), while the lifetime of o-Ps is much longer (142 ns, 3γ self-annihilation). In a matter, a competitive process to the 3γ self-annihilation of o-Ps is the 2γ pick-off annihilation, when the positron annihilates with a surrounding electron of opposite spin instead of annihilation with its bound electron. The pick-off annihilation effectively reduces o-Ps lifetime to several ns and can be easily distinguished in the positron annihilation lifetime spectrum. In conventional metals, Ps is not formed, as any bound state of positron

and electron is quickly destroyed by the screening of conduction electrons [33]. In porous metals, on the contrary, a thermalized positron can escape into a cavity and form Ps by picking an electron on its inner surface [34, 35]. The o-Ps lifetime is then a function of the cavity radius [36, 37]. In the present work, Ps is employed for the characterization of nanoscopic porosity of BAl films.

2. Experimental

Aluminum films were prepared by pulsed DC magnetron sputtering. The target to substrate distance was fixed at 100 mm. The round shape pure Al (99.99 % purity) magnetron target with a diameter of 100 mm was used for sputtering. A DC power supply Hüttinger 3000 combined with a pulse generator MELEC was operated at the power of 400 W, the repetition rate was set to 10 kHz with a duty cycle of 0.5. The base pressure in the chamber of 5×10^{-3} Pa was ensured by the diffusion pump, the magnetron discharge was maintained in N_2/Ar mixture atmosphere at a constant total pressure of 0.5 Pa, which was regulated by a throttle valve at the high-vacuum pump gate. Ar flow was always fixed at 16 sccm, N_2 flow was kept at 0 sccm for the deposition of classic reflective Al (RAl) films, while for the deposition of black Al (BAl) films, it was set to ~0.4 sccm, which corresponds to the N_2 percentage in the N_2/Ar mixture of ~6.5 %. Deposition conditions for all studied Al films are listed in Table 1.

Al film	P_{DC} (W)	U_{DC} (V)	N_2/Ar ratio (%)	thickness (µm)	dep. rate (nm/min)	R_q (nm)	appearance
RAl-1	380	435	0	1.59(4)	80(2)	86	mirror
RAl-2	380	435	0	7.91(2)	61(1)	147	white
BAl-1	350	390	6.0(3)	1.63(2)	82(1)	100	black
BAl-2	350	388	6.5(3)	7.58(6)	58(1)	234	black

Table 1: Deposition conditions (DC supply power, acceleration voltage, N_2/Ar ratio) and basic properties (thickness, roughness R_q, appearance) of reflective and black Al films.

Al films were deposited on amorphous fused silica (FS) substrates with dimensions 10×10 mm^2 and 20×20 mm^2, which were kept at room temperature (RT) during the deposition. In this work, four different Al films are studied: two reflective Al films and two black Al films with thicknesses of ~1.5 µm and ~8 µm. Thicknesses of Al films were determined by contact profilometry (KLA-Tencor P-6 Stylus Profiler).

Al films' surface morphology was investigated by atomic force microscopy (AFM). AFM measurements were carried out at room temperature on an ambient AFM (Bruker, Dimension Icon) in Peak Force Tapping mode with ScanAsyst Air tips (Bruker, k = 0.4 N/m, nominal tip

radius 2 nm) or classical tapping mode using tips Tap 150 Al-g (BudgetSensors, k = 5 N/m, nominal tip radius < 10 nm) for samples with high roughness. Measured topographies have 512 × 512 points^2 resolution. For each film RMS roughness R_q was calculated.

Optical properties were characterized by spectrophotometric reflectance measurements. Specular reflectance (R_{spec}) was measured on a spectrophotometer (PerkinElmer, UV/VIS/NIR Lambda 750) equipped with Universal Reflectance Accessory. A constant angle of incidence of 8° and the range of wavelengths of 190 nm – 1200 nm was used. Diffuse reflectance (R_{diff}) measurements were performed using a spectrophotometer (Analytik Jena, Specord 250) equipped with an integrating sphere for wavelengths range of 320 nm – 1100 nm. A Spectralon (LabSphere) reflectance standard was used as a reference.

X-ray diffraction (XRD) measurements (Rigaku Smartlab, Johansson Ge monochromator, D/teX Ultra250 detector) were performed with Bragg-Brentano geometry using Cu Kα radiation, λ = 1.54051 Å. The crystallite sizes and microstrains were determined using the fundamental approach method [38] implemented in Jana2006 software [39]. The structure was refined using an Al CIF file [40] from the ICSD database, one atomic displacement parameter was refined for all atoms.

Defect structure and nanoporosity were investigated by positron annihilation lifetime spectroscopy (PALS), carried out on a pulsed slow positron beam MePS [41] operating at the ELBE (Electron LINAC with high Brilliance and low Emittance) facility [42] in the Helmholtz-Zentrum Dresden-Rossendorf. The energy of incident positrons in the beam was varied in the range from 1 to 16 keV, which corresponds to the mean positron implantation depth into Al from 15 nm to 1250 nm, as calculated using the Makhovian implantation profile [43]. Positron lifetime spectra were collected using a digital spectrometer [41] with a time resolution of 250 ps (FWHM of the resolution function). The decomposition of positron lifetime spectra into individual exponential components was performed using the PLRF code [44].

3. Results

Studied Al films can be easily distinguished by their appearance. Both BAl exhibit an opaque black surface, while the surface of RAl goes from grey mirror to opaque white with increasing thickness. Contrary to the top surfaces, the bottom surfaces, visible through the transparent FS substrate, are mirror-like for all Al films, see Fig. 1. It testifies that the bottom surface of BAl films attached to the substrate is always a reflective non-porous layer.

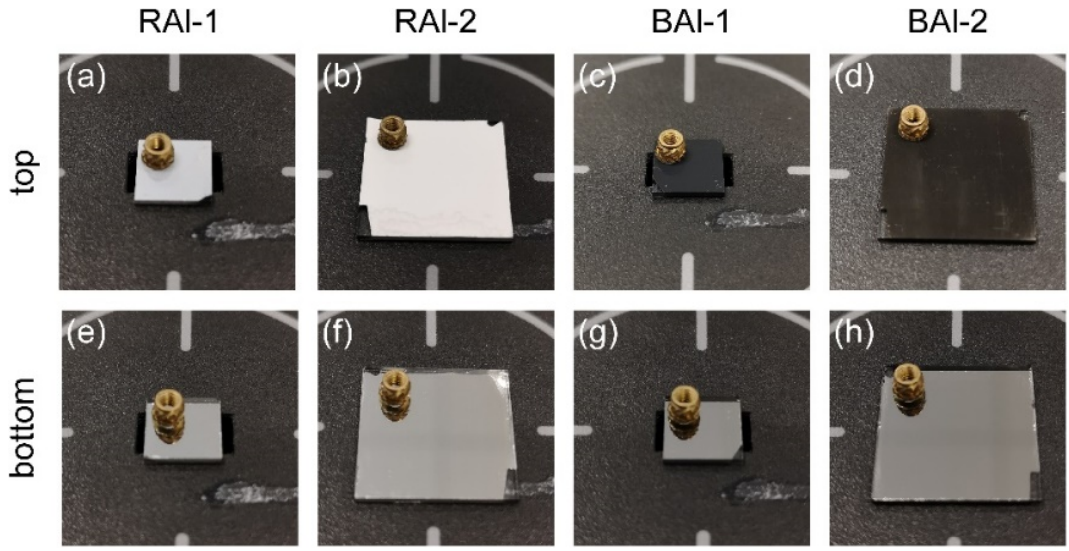

Figure 1: Photos of reflective and black Al films – top and bottom view. A little nut was put onto all samples to illustrate their reflectivity.

The optical properties of Al films can be quantitatively inspected by spectrophotometric reflectance measurements (specular R_{spec} and diffuse R_{diff}), shown in Fig. 2a. Theoretical reflectances of bulk Al with and without a 5 nm thick Al_2O_3 layer, calculated from known optical constants, are included in Fig. 2 as well. The effect of decreasing R_{spec} with increasing film thickness is well demonstrated on reflective RAl-1 and RAl-2 samples. R_{diff} for RAl-1 is always higher than R_{spec}, yet still significantly lower than theoretical values. The typical absorption peak at ~820 nm, caused by interband transitions, is present for all reflective films. Both BAl films exhibit very low values of $R_{spec} < 2$ %, light scattering from the black surface is reflected by enhanced $R_{diff} = 2 – 3$ %, see Fig. 2c. Note that the step at $\lambda = 889$ nm (R_{spec}), visible in Fig. 2c, is an instrumental error caused by the switching of the monochromator. Apparently, this brings a big uncertainty at very low intensities of reflected light with wavelengths $\lambda > 889$ nm.

Bottom layers, Fig. 2b, exhibit substantially higher R_{spec} compared to the Al film surface. No clear thickness effect is observed, however lower R_{spec} for black films implies a different character of both types of Al films rather than different surface properties or crystalline structure only.

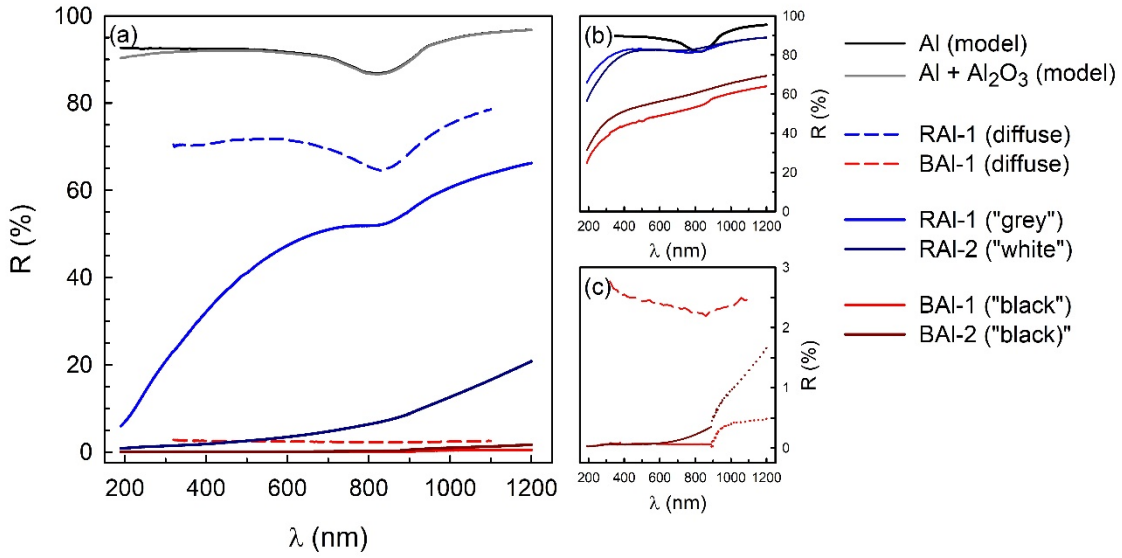

Figure 2: (a) Spectrophotometric specular (R_{spec}, solid lines) and diffuse (R_{diff}, dashed lines) reflectance of reflective and black Al films. Insets show reflectance of bottom surfaces measured through FS substrate (b) and detail for the top surface of black Al (c).

AFM results show a significant difference in the surface morphology of reflective and black films. RAl films exhibit large well-developed grains on the surface with mean sizes estimated to ~600 nm for RAl-1 and ~900 nm for RAl-2, respectively. The surface of black films has a cauliflower-like structure made of smaller surface grains with a mean size estimated to ~100 nm for both BAl-1 and BAl-2. The roughnesses R_q of all films, which are shown in Figs. 3a-d and listed in Table 1, are relatively high and increase with film thickness.

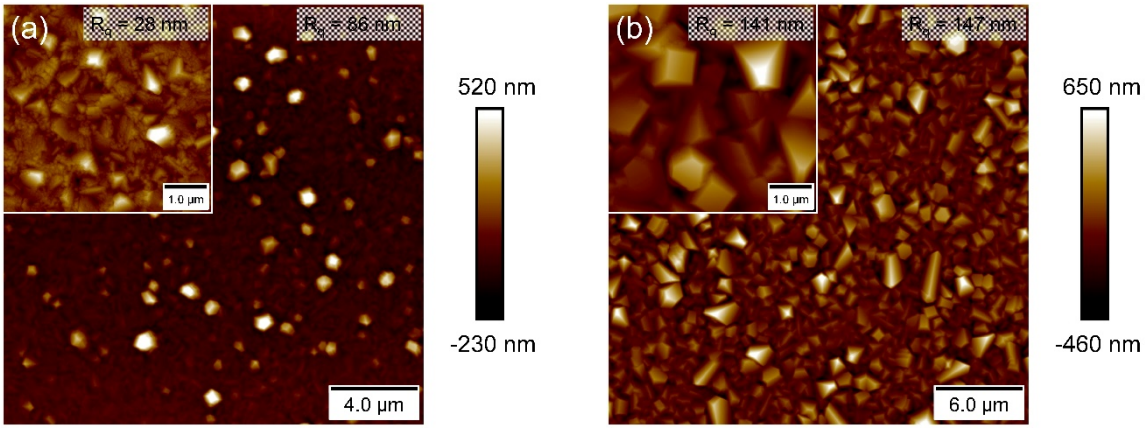

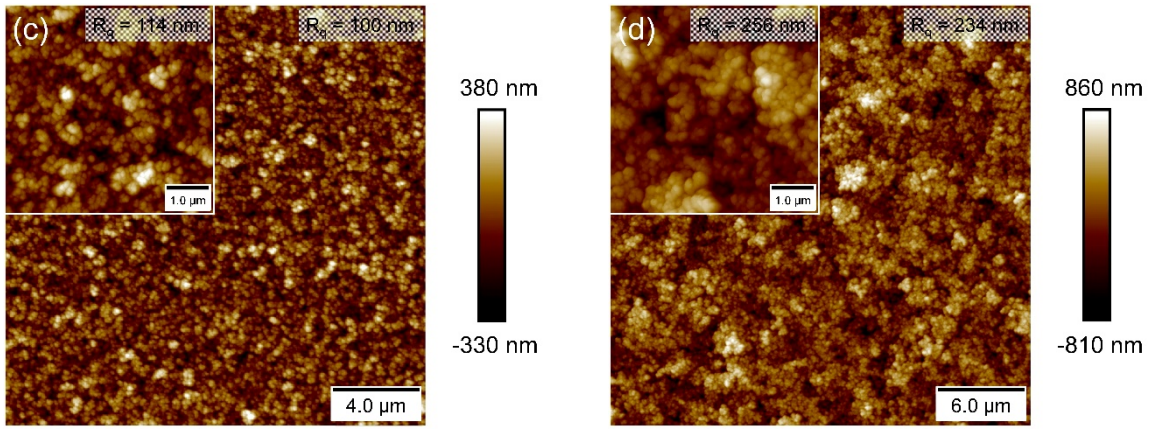

Figure 3: AFM measurements of reflective and black Al films: (a) RAl-1 film (20×20 µm^2 scan), (b) RAl-2 film (30×30 µm^2 scan), (c) BAl-1 film (20×20 µm^2 scan), (d) BAl-2 (30×30 µm^2 scan). Detailed 5×5 µm^2 scans and RMS surface roughnesses R_q are included for each figure.

XRD results are shown in Fig. 4. Despite their different morphology, all Al films crystallize in fcc-Al structure with lattice parameter close to the theoretical value a = 4.0495 Å. No additional crystalline phases, e.g. Al oxide or nitride, were observed. Table 2 shows lattice parameters a_{Al} as well as the mean crystallite size D and microstrains ε for each Al film.

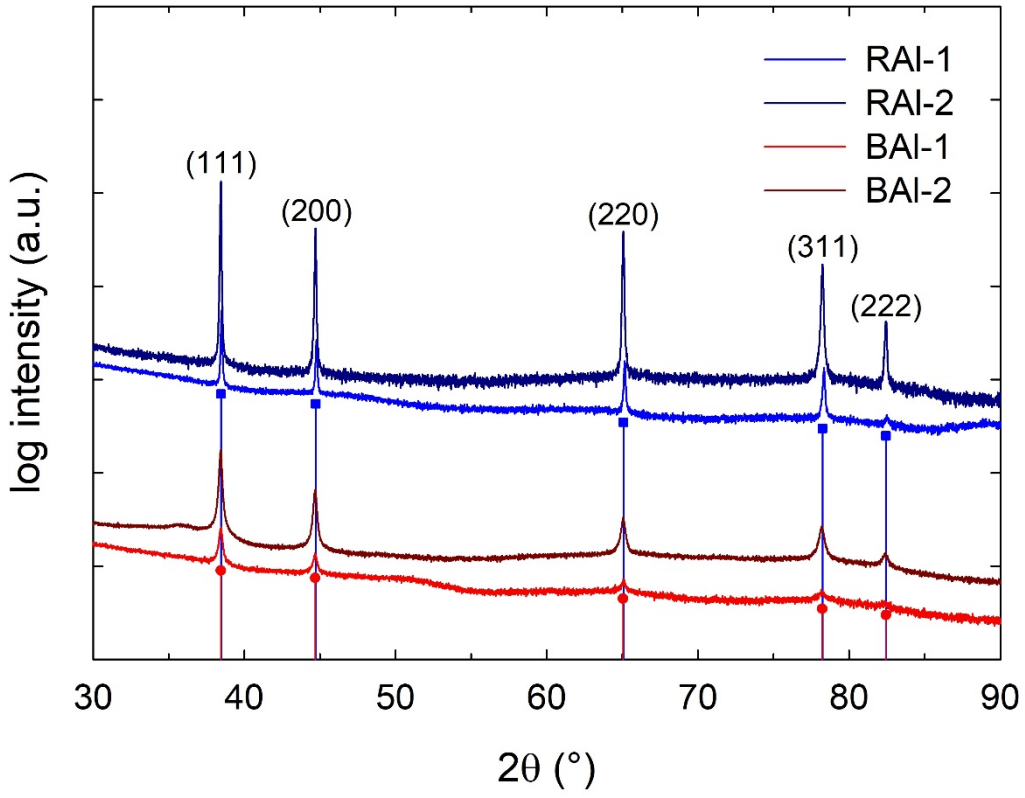

Figure 4: XRD profiles of reflective RAl-1, RAl-2 and black BAl-1, BAl-2 films as measured in Bragg-Brentano θ-2θ geometry. Peak positions are marked with horizontal lines.

Al film	a_{Al} (Å)	D (nm)	ε (%)
RAl-1	4.0452(7)	214(5)	0.11(2)
RAl-2	4.0486(3)	327(7)	0.11(3)
BAl-1	4.051(5)	43(1)	0.23(1)
BAl-2	4.0505(8)	49(2)	0.35(9)

Table 2: Lattice parameters a_{Al}, mean crystallite sizes D, and microstrains ε of reflective and black Al films obtained by XRD analysis.

The defect structure was inspected by positron annihilation lifetime spectroscopy, the results are shown in Fig. 5. According to the positron implantation profile, the maximal positron energies of 9 keV (BAl-1 and RAl-1) and 16 keV (BAl-2 and RAl-2) correspond to the case of 0.3 % and 0.9 % of all positrons penetrating the FS substrate, respectively. Therefore the contribution of the substrate is negligible in PALS measurements. For each positron energy, the positron lifetime spectrum was decomposed into two exponential components: (i) short-lifetime component τ_1 of positrons annihilated as particles, (ii) long-lifetime component τ_2 as a contribution of pick-off annihilations of ortho-positronium (o-Ps). Note that the p-Ps contribution with a lifetime fixed at 125 ps and intensity constrained so that the ratio of o-Ps to p-Ps intensity is 3:1 was included in the model function along with the o-Ps component. Figs. 5a and 5b show positron lifetime τ_1 as a function of energy. The development of o-Ps lifetime τ_2 is shown in Figs. 5c and 5d. Corresponding intensities I_{o-Ps} of o-Ps components are in Figs. 5e and 5f, note that the intensity I_1 of the positron component τ_1 is complementary to the intensity of Ps contribution $I_{Ps} = I_{p-Ps} + I_{o-Ps}$, where $I_{o-Ps}/I_{p-Ps} = 3:1$, according to the formula $I_1 = 100 - I_{Ps}$.

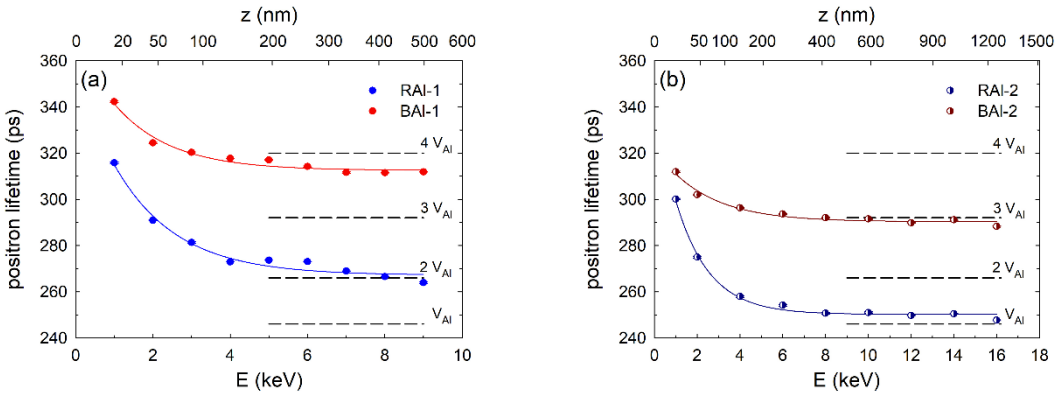

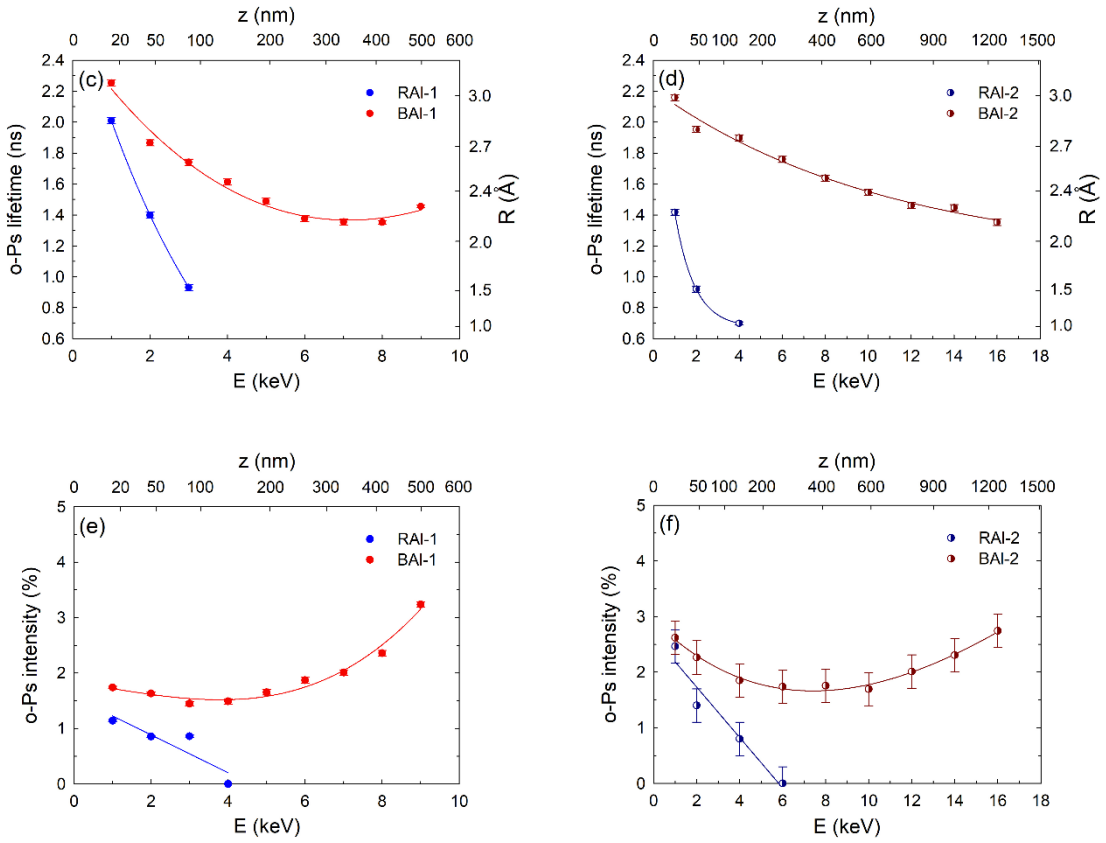

Figure 5: PALS measurements for the reflective (blue points) and black (red points) Al films plotted as a function of the energy of incident positrons: (a,b) lifetime of positron annihilated as a particle, (c,d) o-Ps lifetime, (e,f) o-Ps intensity. The mean positron penetration depth is depicted at the top axis. Pore radius, calculated from the o-Ps pick-off annihilation lifetime using the Tao-Eldrup model [31, 36, 37] is depicted at the right vertical axis in plots (c,d).

The exponential-like decrease of both positron and o-Ps lifetimes in the energy range of 1 – 4 keV is the result of the positron back-diffusion to the surface. Positrons stopped in the sample diffuse in the lattice till they are annihilated or trapped in open volume defects. Some positrons implanted into Al film may reach the film surface by diffusion and be annihilated there.

At the surface, positrons can be either trapped in the surface image potential or may form Ps in the natural Al_2O_3 passivation layer. The probability of positron back diffusion to the surface is given by the positron diffusion length and is gradually decreasing with the energy since with increasing energy positrons are stopped deeper in the film. For energies > 4 keV, virtually all positrons annihilate in the Al film either as particles or in the form of Ps.

4. Discussion

The deposition rates for black and reflective films are comparable for the same thicknesses despite their different growing modes. The decreasing deposition rate as well as the increasing roughness Rq with the film thickness follow the growth process described in [1]. For RAl films the mean grain size increases with the film thickness, see Figs. 3ab and Table 2, according to a V-grow mode. That means small grains grow close to the substrate, following by the competition in the growth between grains and finally by the growth of large grains in top layers. Unlike the RAl, the crystallite size of BAl films seems to be stable and does not depend on the film thickness, see Figs. 3cd and Table 2. This effect is induced by a strong columnar growth favored by the N_2 gas impurity during the deposition step [1]. In this situation, the BAl film coalescence is weak, roughness increases with the thickness, and porosity is expected to be present.

AFM results show that both RAl and BAl exhibit a very rough surface, yet with a completely different morphology. For the same thicknesses, black films exhibit higher roughness than reflective films. However, reflective films need not be always smoother than black films [28, 29, 45]. According to our AFM observations, the roughness of the "white" RAl-2 (thickness 7.91 μm) is higher compared to the "black" BAl-1 (thickness 1.63 μm), for instance. Therefore, we conclude that the surface roughness cannot be considered to be the only key property determining whether the film is black or not.

The optical properties of RAl and BAl can be explained by assuming light reflection from a rough and a porous surface, schematically shown in Fig. 6. On a rough surface, which is characteristic for reflective films, incident light is reflected (scattered) in many directions, multiple reflections are possible. The intensity of light reflected in one specific direction, described by the same angle as the angle of incidence (specular reflection), is substantially lower in comparison with an ideal smooth mirror-like surface. The higher is the roughness, the more significant is the light scattering and the lower is the reflectance R_{spec}. Black films are characterized by a porous surface with a moth-eye-like structure capable of light absorption. Most of the incident light is absorbed by subwavelength electromagnetic interactions with open nanopores [2]. The key factor resolving between the reflective and the black film is, therefore, the presence of fractal-like nanoporosity.

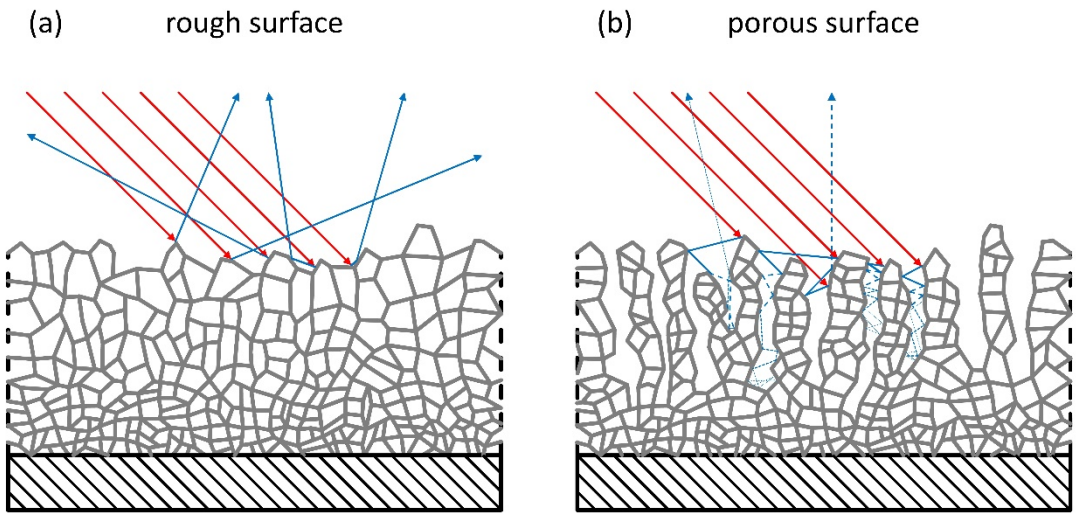

Figure 6: Schematic illustration of light reflection from a rough and porous surface.

High values of microstrain, i.e. local deviations of the lattice parameter, indicate a high density of lattice defects in all films. For RAl, it is likely the consequence of the nanocrystalline structure with a high fraction of grain boundaries. BAl exhibit significantly larger microstrain due to the finer grain structure and/or the presence of another type of open-volume lattice defects.

An insight into the open-volume defect structure was provided by PALS results. In all Al films the positron lifetime τ_1 is substantially higher than the bulk lifetime of defect-free Al of 164 ps [46] and also higher than the lifetime for Al monovacancy of 243 ps [47]. It indicates that positrons are predominantly trapped in defects with a size comparable to small vacancy clusters. Considering the nanocrystalline structure of both types of films, vacancy clusters are most likely located in the grain boundary region. By comparison of the lifetime τ_1 with ab-initio theoretical calculations [48] we obtain that vacancy clusters consist in average of $1-2$ vacancies in RAl and $3-4$ vacancies in BAl, respectively. This is already an indication of a different nature of the grain boundary regions which have more open space in black films. The high density of vacancy nanoclusters is also reflected by extensively high values of microstrain, as measured by XRD. One can see in Table 2 the microstrain is higher in BAl compared to RAl, likely as a consequence of the larger average size of vacancy clusters.

More information can be obtained from the analysis of the pick-off annihilation of o-Ps. One can see in Figs. 5c-f, that in RAl the Ps is formed only on the surface and not inside the film since the intensity of the Ps contribution quickly diminishes with increasing positron energy. This is because the structure of reflective films is compact without porosity and the dominant defects are mono- and divacancies. On the contrary, in black films, the Ps formation takes place not only on the surface but also inside the film. This gives clear evidence that black films contain in addition to small vacancy clusters also nanoporosity.

Employing the Tao-Eldrup model [31, 36, 37], one can calculate the radius of spherical cavities from the o-Ps lifetime measured in the experiment. In BAl, the mean diameter of the cavities is 4 – 5 Å. Nanopores, as described in Fig. 6, likely consist of cavities aligned along grain boundaries, and have one of their dimension significantly longer than the other two. The increasing intensity of the o-Ps component with increasing depth, see Figs. 5ef, is caused by a higher concentration of nanopores consisting of fewer cavities. The mean size calculated according to the Tao-Eldrup model reflects then the minimal dimension of nanopores and is close to the lattice parameter of fcc Al a = 4.0495 Å. As described in [1], the surface of Al grains is passivated by N_2 during the BAl growth. The presence of the passivation layer in the grain boundary region facilitates Ps formation in the cavities.

Diffuse reflectance measurement enables detection of light reflected from the surface in all directions and thus resolve between the light-scattering rough reflective surface and light-absorbing black surface. One can see in Fig. 2 that R_{diff} for the RAl-1 film follows the same dependence as the theoretical reflectance but is lower by approximately 20 %. This is a consequence of the nanocrystalline structure since a high fraction of grain boundaries contributes to the scattering of conduction electrons and shortening of the relaxation time. Hence, according to the Drude-Lorentz model [49], the light absorption is enhanced. For the BAl-1 film, the difference between R_{diff} and R_{spec} is 2 – 3 %, so indeed most of the incident light is absorbed nanoporous film independently on the wavelength.

The same effect of the scattering of conduction electrons on defects was observed for specular reflectance of bottom layers. Note that the light reflection from the FS substrate in the theoretical reflectance model was included. This testifies that the bottom surface of the film attached to the substrate is a smooth layer with a very small roughness.

5. Conclusions

Black aluminum films were deposited by pulsed DC magnetron sputtering using a N_2/Ar gas mixture of ~6.5 %. Positron annihilation spectroscopy was performed to investigate defects and nanoscopic porosity in the film structure. A comparison was carried out between classic reflective and black Al films with thicknesses of ~1.5 µm and ~8 µm. Reflective Al exhibits compact layers with the presence of mono- and divacancies in grain boundary regions. Reflectance is reduced by light scattering from the rough surface. The presence of N_2 in the sputtering gas leads to a change of the growing mode resulting in the black Al film having a moth-eye-like surface morphology with antireflective properties. A large absorbance > 97% of black Al was measured in the wavelength range of 190 nm to 1200 nm. The mean grain size of black Al seems to be stable and independent on the film thickness, unlike the reflective films with a V-grow mode. In addition to vacancy clusters with the mean size of 3 – 4 vacancies, columnar nanopores with a diameter of 4 – 5 Å were observed by positron annihilation lifetime spectroscopy in black Al. The nanoporosity rather than the surface roughness is the

key property of black films. Due to its antireflective properties and extensive surface area, black Al shows a great application potential as a basis for smart absorbers or chemical sensors.

6. Acknowledgments

This work was supported by the Czech Science Foundation (project 18-09347S) and Czech Ministry of Education, Youth and Sports (project SOLID21 CZ.02.1.01/0.0/0.0/16_019/0000760). P. Hruška acknowledges the support of the Czech Academy of Sciences (PPLZ project 100102001). The MePS facility has partly been funded by the Federal Ministry of Education and Research (grant PosiAnalyse 05K2013).

References

1. More-Chevalier, J., et al., *Fabrication of black aluminium thin films by magnetron sputtering.* RSC Advances, 2020. **10**(35): p. 20765-20771.
2. Zhang, X.-Y., et al., *Silver nanoplate aggregation based multifunctional black metal absorbers for localization, photothermic harnessing enhancement and omnidirectional light antireflection.* Journal of Materials Chemistry C, 2018. **6**(5): p. 989-999.
3. Pfund, A.H., *Bismuth Black and Its Applications.* Review of Scientific Instruments, 1930. **1**(7): p. 397-399.
4. Lysenko, V.S. and A.F. Mal'nev, *Optical characteristics of metal blacks.* Journal of Applied Spectroscopy, 1969. **10**(5): p. 566-570.
5. Palatnik, L.S., et al., *Investigation of low vacuum condensates of aluminum using electron microscopy and spectroscopy.* Journal of Applied Spectroscopy, 1977. **27**(6): p. 1524-1526.
6. Anderson, R.E. and J.R. Crawford, *Aluminum black films.* Appl Opt, 1981. **20**(12): p. 2041-2.
7. Novotný, M., et al., *Patent number 307110*. 2017: Czech Republic.
8. Alvarez, R., et al., *Growth regimes of porous gold thin films deposited by magnetron sputtering at oblique incidence: from compact to columnar microstructures.* Nanotechnology, 2013. **24**(4): p. 045604.
9. Mills, A., *Porous Platinum Morphologies: Platinised, Sponge and Black.* Platinum Metals Review, 2007. **51**(1): p. 52-52.
10. Gu, S., et al., *A droplet-based microfluidic electrochemical sensor using platinum-black microelectrode and its application in high sensitive glucose sensing.* Biosens Bioelectron, 2014. **55**: p. 106-12.
11. Fernandez, R.E., et al., *Platinum black electrodeposited thread based electrodes for dielectrophoretic assembly of microparticles.* Biomicrofluidics, 2016. **10**(3): p. 033101.
12. Christiansen, A.B., et al., *Black metal thin films by deposition on dielectric antireflective moth-eye nanostructures.* Sci Rep, 2015. **5**: p. 10563.
13. Toor, F., et al., *Metal assisted catalyzed etched (MACE) black Si: optics and device physics.* Nanoscale, 2016. **8**(34): p. 15448-66.
14. Novotný, M., et al., *Pulsed laser treatment of gold and black gold thin films fabricated by thermal evaporation.* Central European Journal of Physics, 2009. **7**(2).

15. Vorobyev, A.Y. and C. Guo, *Metallic Light Absorbers Produced by Femtosecond Laser Pulses.* Advances in Mechanical Engineering, 2010. **2**: p. 452749.
16. Huang, H., L.M. Yang, and J. Liu. *Femtosecond fiber laser based metal blackening*. in *Nanophotonics and Macrophotonics for Space Environments Vii*. 2013. SPIE.
17. Zheng, B., et al., *Fabrication of broadband antireflective black metal surfaces with ultra-light-trapping structures by picosecond laser texturing and chemical fluorination.* Applied Physics B, 2016. **122**(6): p. 180.
18. Wang, C.M., et al., *Microstructure and absorption property of silver-black coatings.* Japanese Journal of Applied Physics Part 1-Regular Papers Short Notes & Review Papers, 2000. **39**(2a): p. 551-554.
19. Bae, K., et al., *Flexible thin-film black gold membranes with ultrabroadband plasmonic nanofocusing for efficient solar vapour generation.* Nature Communications, 2015. **6**: p. 10103.
20. Moreau, A., et al., *Controlled-reflectance surfaces with film-coupled colloidal nanoantennas.* Nature, 2012. **492**(7427): p. 86-9.
21. Qiu, J. and W.D. Wei, *Surface Plasmon-Mediated Photothermal Chemistry.* The Journal of Physical Chemistry C, 2014. **118**(36): p. 20735-20749.
22. More-Chevalier, J., et al., *Black aluminum-coated Pt/Pb(Zr0.56Ti0.44)O3/Pt thin film structures for pyroelectric energy harvesting from a light source.* Journal of Applied Physics, 2019. **126**(21).
23. Vorobyev, A.Y. and C. Guo, *Colorizing metals with femtosecond laser pulses.* Applied Physics Letters, 2008. **92**(4).
24. Ou, Z., M. Huang, and F. Zhao, *Colorizing pure copper surface by ultrafast laser-induced near-subwavelength ripples.* Optics Express, 2014. **22**(14): p. 17254-65.
25. Huang, H., et al., *Blackening of metals using femtosecond fiber laser.* Appl Opt, 2015. **54**(2): p. 324-33.
26. Vorobyev, A.Y. and C. Guo, *Multifunctional surfaces produced by femtosecond laser pulses.* Journal of Applied Physics, 2015. **117**(3).
27. Melikhova, O., et al., *Positron annihilation study of cavities in black Au films.* Journal of Physics: Conference Series, 2017. **791**.
28. Melikhova, O., et al., *Microstructure and Nanoscopic Porosity in Black Pd Films.* Acta Physica Polonica A, 2020. **137**(2): p. 222-226.
29. Melikhova, O., et al., *Study of Nanoscopic Porosity in Black Metals by Positron Annihilation Spectroscopy.* Acta Physica Polonica B, 2020. **51**(1).
30. O'Neill, P., A. Ignatiev, and C. Doland, *The dependence of optical properties on the structural composition of solar absorbers: Gold black.* Solar Energy, 1978. **21**(6): p. 465-468.
31. Tao, S.J., *Positronium Annihilation in Molecular Substances.* The Journal of Chemical Physics, 1972. **56**(11): p. 5499-5510.
32. Gidley, D.W., H.-G. Peng, and R.S. Vallery, *Positron Annihilation as a Method to Characterize Porous Materials.* Annual Review of Materials Research, 2006. **36**(1): p. 49-79.
33. Seeger, A. and F. Banhart, *On the Systematics of Positron Lifetimes in Metals.* Physica Status Solidi (a), 1987. **102**(1): p. 171-179.
34. Hodges, C.H. and M.J. Stott, *Positrons in metals with voids, vacancies and surfaces.* Solid State Communications, 1973. **12**(11): p. 1153-1156.

35. Čížek, J., et al., *Positronium Formation in Nanostructured Metals.* Acta Physica Polonica A, 2017. **132**(5): p. 1579-1584.
36. Eldrup, M., D. Lightbody, and J.N. Sherwood, *The temperature dependence of positron lifetimes in solid pivalic acid.* Chemical Physics, 1981. **63**(1-2): p. 51-58.
37. Ito, K., H. Nakanishi, and Y. Ujihira, *Extension of the Equation for the Annihilation Lifetime ofortho-Positronium at a Cavity Larger than 1 nm in Radius.* The Journal of Physical Chemistry B, 1999. **103**(21): p. 4555-4558.
38. Cheary, R.W., A.A. Coelho, and J.P. Cline, *Fundamental Parameters Line Profile Fitting in Laboratory Diffractometers.* J Res Natl Inst Stand Technol, 2004. **109**(1): p. 1-25.
39. Petříček, V., M. Dušek, and L. Palatinus, *Crystallographic Computing System JANA2006: General features.* Zeitschrift für Kristallographie - Crystalline Materials, 2014. **229**(5).
40. Bourbia, A., et al., *X-ray and optical crystallographic parameters investigations of high frequency induction melted Al-(alpha-Al(2)O(3)) alloys.* J Xray Sci Technol, 2010. **18**(2): p. 201-19.
41. Wagner, A., et al., *Positron annihilation lifetime and Doppler broadening spectroscopy at the ELBE facility* AIP Conference Proceedings, 2018. **1970**: p. 040003
42. Gabriel, F., et al., *The Rossendorf radiation source ELBE and its FEL projects.* Nuclear Instruments and Methods in Physics Research Section B: Beam Interactions with Materials and Atoms, 2000. **161-163**: p. 1143-1147.
43. Schultz, P.J. and K.G. Lynn, *Interaction of positron beams with surfaces, thin films, and interfaces.* Reviews of Modern Physics, 1988. **60**(3): p. 701-779.
44. Čížek, J., *PLRF Code for Decomposition of Positron Lifetime Spectra.* Acta Physica Polonica A, 2020. **137**(2): p. 177-187.
45. Melikhova, O., et al., *Positron annihilation study of cavities in black Au films.* Journal of Physics: Conference Series, 2017. **791**: p. 012018.
46. Čížek, J., et al., *Using of Modified Trapping Model in Positron-Lifetime Study of Cold-Worked Aluminium.* physica status solidi (a), 2000. **180**(2): p. 439-458.
47. Fluss, M.J., et al., *Measurements of the vacancy formation enthalpy in aluminum using positron annihilation spectroscopy.* Physical Review B, 1978. **17**(9): p. 3444-3455.
48. Čížek, J., et al., *Vacancy clusters in ultra fine grained metals prepared by severe plastic deformation.* Journal of Physics: Conference Series, 2013. **443**.
49. Marković, M.I. and A.D. Rakić, *Determination of optical properties of aluminium including electron reradiation in the Lorentz-Drude model.* Optics & Laser Technology, 1990. **22**(6): p. 394-398.